Towards Infrared Spectral Extension of CMOS Image Sensors

Kaitlin M. Anagnost, Xiaoxin Wang, Jifeng Liu, and Eric R. Fossum
Thayer School of Engineering, Dartmouth College, Hanover, NH, USA
Contact: Kaitlin.Anagnost.TH@dartmouth.edu

Abstract

A new structural integration scheme for p-type infrared (IR) absorbers directly on silicon (Si)-based CMOS image sensors with type-II band alignment is proposed and explored by calculation as an alternative to HgCdTe and other hybridized IR detectors. While HgCdTe is a material of choice for many IR detectors, its challenging manufacturing process and thermal reliability, among other factors, prove detrimental to some applications. Si-based sensors with directly deposited IR absorbing layers may be a suitable alternative. The band structures for the IR absorbing materials $Ge_{0.89}Sn_{0.11}$ and $In_{0.1}Ga_{0.9}Sb$ on Si are calculated and analyzed. Detector parameters including dark current, target wavelength, quantum efficiency (QE), and others, are also calculated to explore this approach in concert with separate experimental fabrication and measurement.

Keywords—CMOS image sensor, Non-visible, Spectral extension, IR.

Introduction

There is a desire to transition towards Si-based IR sensors due to easier readout, potentially lower readout noise, and other circuit integration on-chip. Further, they are expected to avoid the manufacturing, scalability, and thermal reliability challenges HgCdTe and other hybrid sensors face. However, without an IR absorption layer, Si has a weak IR response because of its 1.12 eV bandgap [1]. IR imaging has many uses, including in light detection and ranging, security, medical, and more.

A new structural integration scheme for p-type infrared (IR) absorbers directly on silicon (Si)-based CMOS image sensors (CIS) with type-II band alignment is proposed and explored by calculation as an alternative to state-of-the-art hybrid IR detectors. In the proposed sensor, photons strike a p-type IR absorption layer that forms a type-II heterostructure on Si, generating photoelectrons that diffuse into the pixel's n-type Si storage well, leaving the holes in the p^+ Si pinning region. Depositing the IR absorber directly on silicon negates the need for metal hybrid bonds or bump bonds typically used in many IR detectors. Aside from reliability concerns during thermal cycling and yield, a metal interconnect implies a 3-T type readout with residual kTC noise and potential lag. Direct injection of photoelectrons into Si permits low-noise 4-T readout.

$Ge_{0.89}Sn_{0.11}$ and $In_{0.1}Ga_{0.9}Sb$ are considered as possible materials for the IR absorption layer. Like HgCdTe, GeSn has a direct, tunable bandgap, but is CMOS- and Si-compatible, and thus more scalable [2]–[4]. Experimental results in [5] verify proof-of-concept with 100 mA/W responsivity at ~2 µm compatible with back-end-of-line CMOS processing. III-V materials like InGaSb also have direct bandgaps [6] and are easier to manufacture than II-VI compounds [7].

To advance this approach towards use on a CIS, the electron diffusion and subsequent readout is first optimized via an interdigitated structure. Deposition layer thickness, minimum interdigitated structure width, target wavelength, quantum efficiency, and dark current are then calculated to further characterize the proposed device.

Band Structure Calculation and Analysis

Some photoelectrons will diffuse to locations that won't be readout if the IR absorber is deposited over the entire p+ Si pinning layer commonly used in frontside-illuminated devices. Therefore, an interdigitated Si layer with p+ and n type regions, equivalently a partial pinning layer, is considered as shown in Figure 1. This can be implemented with an interdigitated mask for p+ pinning layer implantation.

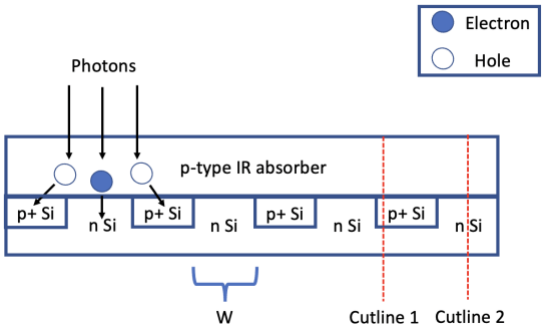

Figure 1. IR-absorbing layer on interdigitated silicon layer.

The IR-absorber/Si band structures are calculated using the Anderson approach, which utilizes the vacuum level to find the valence band offset. The difference in conduction band energies ΔE_c is the difference between the Si and IR absorbers' affinities, $q\chi_{Si}$ and $q\chi_{absorber}$, respectively. Using the direct bandgap of the IR absorber and indirect bandgap of Si (1.12 eV), we find the difference in IR absorber and Si bandgaps ΔE_g and thus valence band energies ΔE_v:

$$\Delta E_v = \Delta E_g - \Delta E_c \quad (1)$$

Assuming Si's vacuum level is $q\chi_{Si}$ = 4.05 eV, since $E_c = E_v + E_g$, we can determine Si's E_c and E_v, and use $\Delta E_v, \Delta E_c$, and ΔE_g to find those of the absorbers.

To calculate the Fermi level E_F, the density of states in the conduction band N_c and valence band N_v are first found using (2.13a) and (2.13b) on pp. 51 in [8]. The intrinsic Fermi level E_i and intrinsic carrier concentration n_i are then determined via (2.36) on pp. 62 and (2.21) on pp. 55 in [8], respectively. Finally, E_F is calculated using 2.38a and 2.38b on pp. 63 in [8].

The depletion region widths on each side of the junction are found next using (143a) and (143b) in [9]. The Debye lengths L_D are subsequently determined and compared to the depletion widths to validate the analyses.

The band bending present in the IR absorbers and Si are found next. The sum of the interface potentials for the absorber and Si, $q\psi_{absorber} + q\psi_{Si} = q\psi_{bi}$ and with 0 V applied, are related by (15a) and (15b) on pp. 82 of [9]. The Fermi levels of the materials are then aligned at 0 eV for simplicity.

The equilibrium band diagrams for the crosscuts of Fig. 1 were calculated with the results using $Ge_{0.89}Sn_{0.11}$ and $In_{0.1}Ga_{0.9}Sb$ shown in Fig. 2 and 3, respectively. As illustrated, the p+ Si regions in Figure 2a and 3a serve as a potential barrier against photoelectron transport but collect holes generated in the IR absorber. Conversely, the p-type IR absorber/n-type heterostructure allows electron diffusion to the n-well, as depicted in Fig. 2b and 3b. The $Ge_{0.89}Sn_{0.11}$/n Si conduction band structure has no barrier for electron diffusion from $Ge_{0.89}Sn_{0.11}$ to n Si, while the $In_{0.1}Ga_{0.9}Sb$/Si conduction band has a small barrier that allows electrons to tunnel to the n Si well. $Ge_{0.89}Sn_{0.11}$ is thus more suited to this design as an IR absorbing layer.

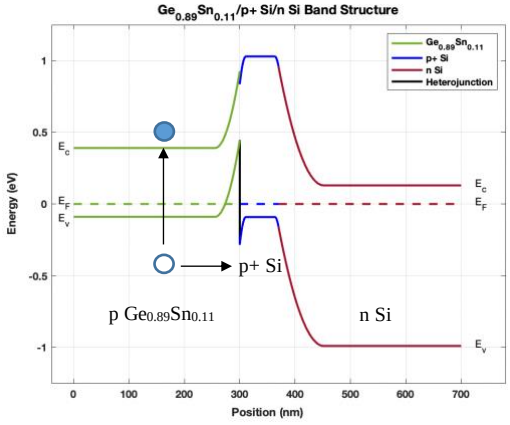

(a)

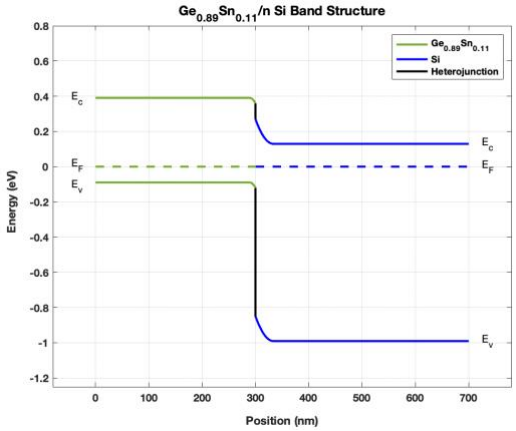

(b)

Figure 2. *Calculated band structure for $Ge_{0.89}Sn_{0.11}$ for (a) Cutline 1 and (b) Cutline 2 in Figure 1.*

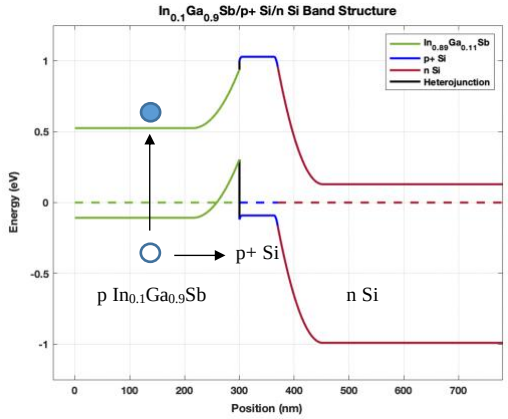

(a)

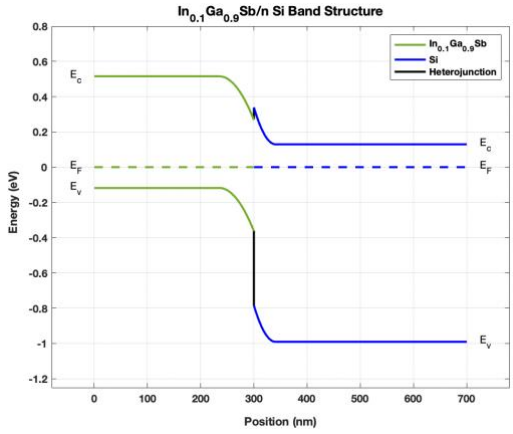

(b)

Figure 3. *Calculated band structure for $In_{0.1}Ga_{0.9}Sb$ (a) Cutline 1 and (b) Cutline 2 in Figure 1.*

QE Estimation

Deposition layer thickness, minimum interdigitated structure width, target wavelength, and QE are evaluated next to obtain a greater understanding of the device.

The ideal deposition thickness of the materials are first found using Beer-Lambert's law [10]

$$I = I_0 e^{-\alpha z} \tag{2}$$

where z is the material's depth, α is the absorption coefficient, and I_0 is the initial intensity.

The ratio of the amount of light absorbed and readout to the total amount of light incident on the material, or external quantum efficiency (EQE), is

$$EQE = A \times CP \tag{3}$$

where A is the amount of incident light absorbed in the device and CP is the collection probability, or probability that the light will be readout and is given by 8.13 in [11] as

$$CP = e^{-x/L_D} \tag{4}$$

where x is the distance from the depletion region and L_D is the minority carrier diffusion length. Light absorbed within the depletion region has a 100% probability of being collected in the absence of a potential barrier. However, the CP for light outside the depletion region exponentially decreases with distance from the depletion region. As a result,

$$EQE = A_{out} \times CP + A_{depl} \tag{5}$$

where A_{out} and A_{depl} are the percentages of light absorbed outside and inside of the depletion region, respectively. A_{depl} is given by

$$A_{depl} = e^{-\alpha(z - w_{depl})} - e^{-\alpha z} \tag{6}$$

with no potential barrier present. In the presence of a potential barrier, A_{depl} becomes $A_{depl} \times$ T, the tunneling probability.

Since the CP varies as a function of length, A_{out} must be calculated for each position used. Using (2),

$$A_{out} = \sum_{i=1}^{i=1000} (e^{-\alpha z_{i-1}} - e^{-\alpha z_i}) \tag{7}$$

where i is the bin number, $z_i = (z - w_{depl})(i)(\Delta z_i)$, $\Delta z_i = 0.001$, and w_{depl} is the depletion region width. The absorption in each bin is subtracted from the previous one so the value isn't cumulative. The EQE is then found, with the results displayed in Table 1.

The ratio of the number of carriers readout to the number of photons absorbed, or the internal quantum efficiency (IQE), can also be compared between the materials. For $Ge_{0.89}Sn_{0.11}$, the IQE is simply given by the collection probability CP, while the IQE for $In_{0.1}Ga_{0.9}Sb$ is CP × T due to the potential barrier.

The refractive index is subsequently calculated, and the minimum interdigitated structure width is found using Snell's law, with the results shown in Table 1.

Dark Current Estimation

The dark current is critical, especially in low-light conditions in which the photo signal may become overwhelmed by the noise. It is first calculated at 300 K and using 100 mV reverse bias. Only the variables and equations for electrons will be stated to avoid redundancy, with the equivalent expression for holes left to the reader.

First the electron concentration n of the IR absorber is determined from 2.16a in [20]:

$$n = N_C e^{(E_F - E_C)/kT} \tag{8}$$

The change in electron concentration with respect to time, $\frac{\partial n}{\partial t}$, at the IR absorber/Si interface is given by (5) in [12] and is the dark current in this device

$$\frac{\partial n}{\partial t} = \frac{1}{q}\frac{d}{dx} J_n - R_{bb} - R_{nt} \tag{9}$$

where J_n is the electron current density, R_{bb} is the band-to-band recombination term, and R_{nt} is the transition rate from traps to the conduction band. From (8) in [12]:

$$J_n = qn\mu_n E + qD_n \nabla n \tag{10}$$

where μ_n is the electron mobility, E is the electric field, and D_n is the diffusion constant in an n-type semiconductor.

The band-to-band recombination coefficient is

$$R_{bb} = B_r(np - n_i^2) \tag{11}$$

where B_r is the recombination coefficient [13], [14] (19), (Appendix C). The transition rate from traps to the conduction band, R_{nt}, from [13] (8, 10), is

$$R_{nt}(x) = \int_{E_v}^{E_c} r_{nt}(E_t, x) dE_t \tag{12}$$

E_t is the trap energy and r_{nt} is the transition rate from traps at particular energy levels to the conduction band [13] (9, 11)

$$r_{nt}(E_t) = c_n n(1 - f_t) D_t - e_n f_t D_t \tag{13}$$

where c_n is the electron capture coefficient, f_t is the occupation function, D_t is the defect density of states, and e_n is the electron thermal emission rate. $\frac{\partial n}{\partial t}$ is then

found, with the results shown in Table 1.

Results

As illustrated in Table 1, $Ge_{0.89}Sn_{0.11}$'s target wavelength extends farther into the IR regime due to its smaller bandgap. The minimum interdigitated width for the structures isn't a concern because of the IR absorbing layer's thickness. $In_{0.1}Ga_{0.9}Sb$'s EQE and IQE are low because the potential barrier in its conduction band

hinders electron transport to the Si. $Ge_{0.89}Sn_{0.11}$ has more dark current because its smaller bandgap allows carriers to jump into the conduction and valence bands with less energy than in materials with larger bandgaps like $In_{0.1}Ga_{0.9}Sb$. To achieve 1 pA/cm^2 dark current with 100 mV reverse bias, $Ge_{0.89}Sn_{0.11}$ and $In_{0.1}Ga_{0.9}Sb$ would need to be cooled to 155 K and 185 K, respectively, assuming mid-gap defect state excitation at the heterojunction interface dominates the thermal generation process over that of band-to-band processes.

Parameter	$Ge_{0.89}Sn_{0.11}$	$In_{0.1}Ga_{0.9}Sb$
IR Absorber Bandgap	0.48 eV	0.63 eV
Wavelength Range	0.4-2.1 um	0.4-2.0 um
IR Absorber Thickness	100 nm	100 nm
External Quantum Efficiency	23%	0.9%
Internal Quantum Efficiency	~100%	~10%
Minimum Interdigitated Width	48 nm	52 nm
Eff. Trap Density incl. heterojunction interface	1x10^{17}/cm^3	1x10^{16}/cm^3
Dark current at 300 K, 100 mV reverse bias	12.6 mA/cm^2	0.22 mA/cm^2
Temp. for 1 pA/cm^2 dark current	155 K	185 K
Potential Readout Noise (4T config.)	<5e- rms	<5e- rms

Table 1. *Simulated parameters of the proposed detector.*

Discussion

From these calculations, a better understanding of the detector is formed. The results indicate that $Ge_{0.89}Sn_{0.11}$ is more promising than $In_{0.1}Ga_{0.9}Sb$ to allow photoelectron diffusion into the Si. $Ge_{0.89}Sn_{0.11}$ extends the detector's spectral responsivity farther into the IR range with higher QE, but at the cost of higher dark current. Future work includes depositing the $Ge_{0.89}Sn_{0.11}$ on Si-based CMOS image sensors and testing them. If successful, the widespread use of Si-based IR detectors will be closer to being in reach.

Acknowledgments

KA appreciates the support of the Dartmouth PhD Innovation Program. This research has also been partially supported by the Air Force Office of Scientific Research under the award number FA9550-19-1-0341 managed by Dr. Gernot Pomrenke.

References

[1] A. Rogalski, "HgCdTe infrared detector material: History, status and outlook," *Reports on Progress in Physics*, 2005, doi: 10.1088/0034-4885/68/10/R01.

[2] D. Zhang *et al.*, "High-responsivity GeSn short-wave infrared p-i-n photodetectors," *Applied Physics Letters*, 2013, doi: 10.1063/1.4801957.

[3] H. Tran *et al.*, "Si-Based GeSn Photodetectors toward Mid-Infrared Imaging Applications," *ACS Photonics*, 2019, doi: 10.1021/acsphotonics.9b00845.

[4] R. Soref, D. Buca, and S.-Q. Yu, "Group IV Photonics: Driving Integrated Optoelectronics," *Optics and Photonics News*, 2016, doi: 10.1364/opn.27.1.000032.

[5] X. Wang *et al.*, "GeSn on Insulators (GeSnOI) Toward Mid-infrared Integrated Photonics," *Frontiers in Physics*, vol. 7, 2019, Accessed: Dec. 01, 2022. [Online]. Available: https://www.frontiersin.org/articles/10.3389/fphy.2019.00134

[6] S. P. Svensson, W. A. Beck, W. L. Sarney, D. Donetsky, S. Suchalkin, and G. Belenky, "Temperature dependent Hall effect in InAsSb with a 0.11 eV 77 K-bandgap," *Appl. Phys. Lett.*, vol. 114, no. 12, p. 122102, Mar. 2019, doi: 10.1063/1.5081120.

[7] E. H. Steenbergen, C. P. Morath, D. Maestas, G. D. Jenkins, and J. V. Logan, "Comparing II-VI and III-V infrared detectors for space applications," in *Infrared Technology and Applications XLV*, SPIE, May 2019, pp. 299–307. doi: 10.1117/12.2519250.

[8] R. Pierret, *Semiconductor Device Fundamentals*. Addison-Wesley Publishing Company, 1996.

[9] S. M. Sze and K. K. Ng, "Physics of Semiconductor Devices, 3rd Edition - Simon M. Sze, Kwok K. Ng," *Physics of Semiconductor Devices, 3rd Edition.; John Wiley & Sons, Inc.; NJ*, 2007.

[10] "Brown and Arnold - 2010 - Fundamentals of Laser-Material Interaction and App.pdf." Accessed: Feb. 22, 2022. [Online]. Available: https://spikelab.mycpanel.princeton.edu/papers/book02.pdf

[11] "Solar cells—Operating principles, technology and system applications," in *Solar Energy*, 1982, p. 447. doi: 10.1016/0038-092X(82)90265-1.

[12] B. Baert, M. Schmeits, and N. D. Nguyen, "Study of the energy distribution of the interface trap density in a GeSn MOS structure by numerical simulation of the electrical characteristics," *Applied Surface Science*, vol. 291, pp. 25–30, Feb. 2014, doi: 10.1016/j.apsusc.2013.09.022.

[13] M. Sakhaf and M. Schmeits, "Capacitance and conductance of semiconductor heterojunctions with continuous energy distribution of interface states," *Journal of Applied Physics*, vol. 80, no. 12, pp. 6839–6848, Dec. 1996, doi: 10.1063/1.363750.

[14] W. Dou, "High-Sn-content GeSn Alloy towards Room-temperature Mid Infrared Laser," University of Arkansas, Fayetteville.